JOURNAL OF THEORETICAL AND APPLIED MECHANICS
61, 1, pp. 129-146, Warsaw 2023
https://doi.org/10.15632/jtam-pl/157462

RESEARCH ON VIBRATION EVOLUTION OF A BALL BEARING WITHOUT THE CAGE UNDER LOCAL VARIABLE-DIAMETER RACEWAY DAMAGE

Enwen Zhou, Yanling Zhao, Huanqing Zhang

Key Laboratory of Advanced Manufacturing Intelligent Technology Ministry of Education, Harbin University of Science and Technology, Harbin, China

Corresponding author Yanling Zhao, e-mail: ztgsci1118@163.com

This article presents an analysis of vibration evolution of a ball bearing without the cage. A vibration model in which time-varying displacement, time-varying stiffness, contact force and collision force are comprehensively considered, is proposed. On this basis, the law of motion of the bearing is studied. It is shown that a variable-diameter raceway affects the radius of curvature, which effects the dispersion of rolling elements. The damaged variable--diameter raceway leads to discrete failure, contact force and collision force of rolling elements, which are main reasons that cause vibration mutation. The bearing motion changes from quasi-periodic to chaotic motion.

Keywords: ball bearing, vibration evolution, variable-diameter raceway, damage

1. Introduction

Rolling bearings are one of the essential supporting parts in rotating machinery. Severe friction and collision between the cage and the rolling element will make the bearing significantly warm up in a short time. Therefore, a ball bearing without the cage plays an important role in the field of high precision machinery instead of a traditional bearing. However, the designed local variable-diameter raceway of a ball bearing without the cage can realize automatic discretization of rolling elements. It can reduce wear and vibration caused by random collisions. High frequency contact between a rolling element and the variable-diameter raceway is the main reason for an increase of vibration. The damaged variable-diameter raceway leads to collision and discrete failure of rolling elements (Zhao *et al.*, 2021, 20221).

Although a large number of scholars studied the influence of the bearing damage model on vibration characteristics, vibration behavior caused by different damage forming factors is far from being well understood. McFadden and Smith (1984) considered the influence of geometric shape, rotational speed, contact load, acceleration sensor sensitivity, vibration attenuation and other factors. The local damage induced by a pulse excitation is simplified. The influence of damage on vibration characteristics of bearings was studied. Fan *et al.* (2017) considered additional contact deformation caused by the inner and outer ring damage combined with bearing damage and bearing seat in the horizontal direction under an unbalanced force. Eight degrees of freedom vibration differential equation was established. Behzad *et al.* (2011) believed that the form of bearing damage was a random variation of the roughness amplitude in a particular range. Khanam *et al.* (2015) proposed that a periodic pulse generated by bearing damage seriously affects vibration characteristics of the bearing.

Vibration characteristics of bearings are affected by the impact force generated by rolling over the damaged raceway. According to the principle of engineering mechanics, the function

expression of an impact force is established to simulate the response of the bearing seat. A relative importance of variable stiffness and ball mass to the raceway impact was further studied. The elastic deformation of bearing members under a centrifugal force and external load was considered by Liu *et al.* (2019). They analyzed the influence of roll deformation, flange deformation, external load and rotational speed on flexible and rigid vibration. Yang *et al.* (2019) investigated bending-torsional coupling vibration of an aeroengine blade shell tribological dynamic model, which was caused by thermal load. Zheng *et al.* (2021) proposed a dynamic model of a rolling bearing based in an impact system. Considering the collision between the rolling element and damage, they regarded contact between the rolling element and the raceway as a nonlinear spring.

Cui *et al.* (2019) established a dynamic model considering geometrical characteristics and deformation of the rolling element. Vibration response characteristics under different damage sizes were studied. They further deduced a functional relationship between vibration characteristics and damage size. Liu *et al.* (2018) proposed a new bearing vibration model with a notch, which gave a time-varying contact force between the notch and the shoulder. Parmar *et al.* (2021) verified the vibration response law of rolling bearings with local defects and dynamic misalignment by numerical simulation and experiment. Shah and Patel (2019) established mechanical vibration models of deep groove ball bearings under healthy and damaged conditions. A dynamic model of an angular contact ball bearing and floating displacement bearing system was reformulated by Xi *et al.* (2019). They studied the dynamic-frequency response function of a spindle bearing system at different speeds and the time-history response of the spindle bearing system under different cutting forces. Yang *et al.* (2018) analyzed vibration signals of bearings and casings, and established a dynamic model of a nonlinear rolling bearing rotor-bearing-casing system. Liu *et al.* (2022) used Hertz's contact theory and the relative relationship between rolling element and damage to determine the additional contact area. Liu *et al.* (2022) adopted the locomotive--track space coupling dynamic model with traction power transmission to obtain the dynamic vibration response of the system.

There are many studies on damage vibration of bearings. The study of bearing damage is limited to single damage geometry, and most of the papers establish specific dynamic models of bearing damage. At present, few scholars studied vibration characteristics of ball bearings wihout the cage. The vibration effects caused by rolling body collisions are also rarely considered.

In this paper, the vibration evolution model of a ball bearing without the cage under local variable-diameter raceway damage is established. By analyzing dynamic characteristics of rolling elements of a ball bearing without the cage under the condition of local variable-diameter raceway damage, a relationship equation between damage width and discrete spacing of rolling elements is established. This paper analyzes the impact force of the element rolling along a variable--diameter raceway when damage of the variable-diameter raceway occurs. A rolling element impact model is established. Combined with time-varying contact stiffness of the rolling element in the collision model, the bearing vibration equation was established. The vibration law and displacement velocity phase diagram of the bearing inner ring in the time domain and frequency domain are researched. Finally, this paper discusses the vibration evolution law of bearings under different damage degrees of local variable-diameter raceways.

2. Motion analysis of the rolling element under damage

In order to realize automatic discretization of the rolling element, we changed the radius of curvature of the local outer ring, which is defined as the variable-diameter raceway. The change of curvature radius affects rotational speed of the rolling body. The rotational speed of the rolling element decreases when it enters the variable-diameter raceway and increases when it

leaves. This keeps a certain distance between the rolling elements until the variable-diameter raceway is damaged and fails. Figure 1 shows a schematic diagram of a cage free bearing with a local variable-diameter raceway. Periodic motion of the rolling element is the cause of damage of the variable-diameter raceway, which varies in the contact point between the rolling element and the variable-diameter raceway. Contact points e_1 and e_2 expand outwards to e_1' and e_2', respectively. The inner ring extrudes the rolling body outwards, which causes that the junction points p_1 and p_2 between the variable-diameter raceway and the conventional raceway expand to p_1' and p_2'. When the radius of curvature decreases to a certain value with the expansion of damage, the distance between adjacent rolling elements decreases continuously and a collision occurs. This is defined as a discrete failure.

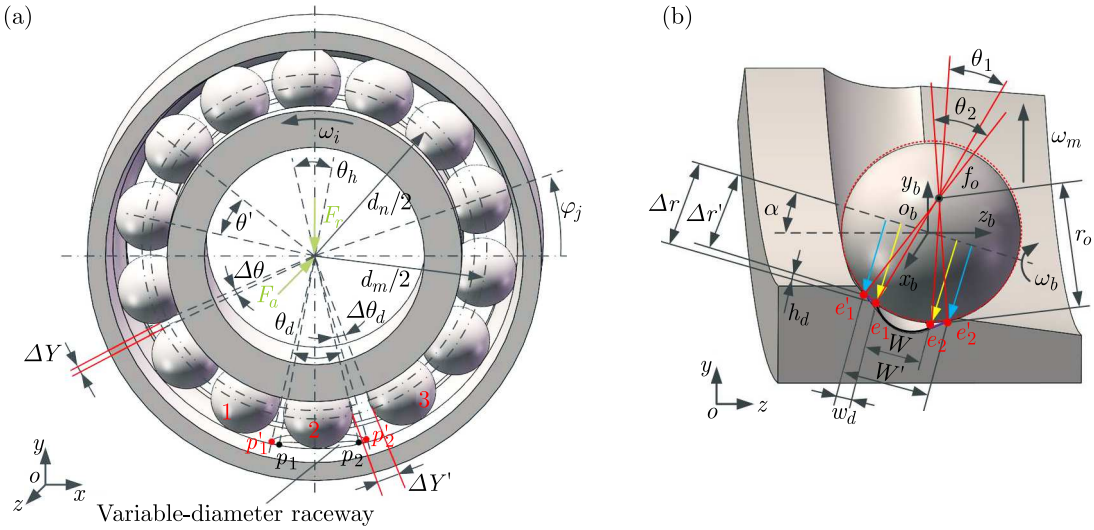

Fig. 1. Diagram of a ball bearing without the cage: (a) variable-diameter raceway structure; (b) rolling element contact

According to geometrical characteristics of the variable-diameter raceway, the circumferential span angle and the discrete spacing of the damaged variable-diameter raceway are obtained

$$\begin{aligned}\theta_d &= \theta_h + 4\arcsin\frac{w_d}{d_m + D_w\cos\alpha}\\ \Delta Y' &= \frac{\pi d_n}{180}\Big(\theta_h + 4\arcsin\frac{w_d}{d_m + D_w\cos\alpha}\Big)\Big(\frac{D_w}{2(\Delta r - h_d)}\Big)\end{aligned} \tag{2.1}$$

where θ_d and θ_h denote circumferential span angle corresponding to the undamaged and damaged variable-diameter raceway, respectively. $\Delta Y'$ is the discrete distance between two rolling element after damage. It can be used as a condition to judge the discrete failure. Damaged width and length of the variable-diameter raceway are respectively expressed as w_d and h_d. D_w is diameter of the rolling element, d_m is diameter of the bearing pitch circle and α is the rolling element contact angle. The radius of rotation is expressed by Δr.

Based on equation $(2.1)_2$, when the variable-diameter raceway is damaged, the discrete spacing parameter that affects the rolling element is mainly the effective radius of gyration. Conventional raceway rolling speed can be expressed as $V_1 = \omega_m d_m/2$, V_2 is the rolling speed of the variable-diameter raceway. Therefore, the velocity difference between adjacent rolling elements ΔV can be calculated from

$$\begin{aligned}V_2 &= \omega_m'\Big(\frac{d_m}{2} + (D_w - \Delta r')\cos\alpha\Big)\\ \Delta V &= \frac{\omega_i d_m}{4}\Big(1 - \frac{D_w}{d_m}\cos\alpha\Big) - \frac{\omega_b \Delta r'\Big((D_w - \Delta r')\cos\alpha + \frac{dm}{2}\Big)}{D_w\cos\alpha + \frac{d_m}{2}}\end{aligned} \tag{2.2}$$

where ω_m and ω'_m are angular velocities in revolution of the conventional and local variable--diameter raceway, respectively. When the variable-diameter raceway is damaged, the corresponding radius of rotation is expressed as $\Delta r'$. ω_i and ω_b are rotational angular velocities of the inner ring and rolling element, respectively.

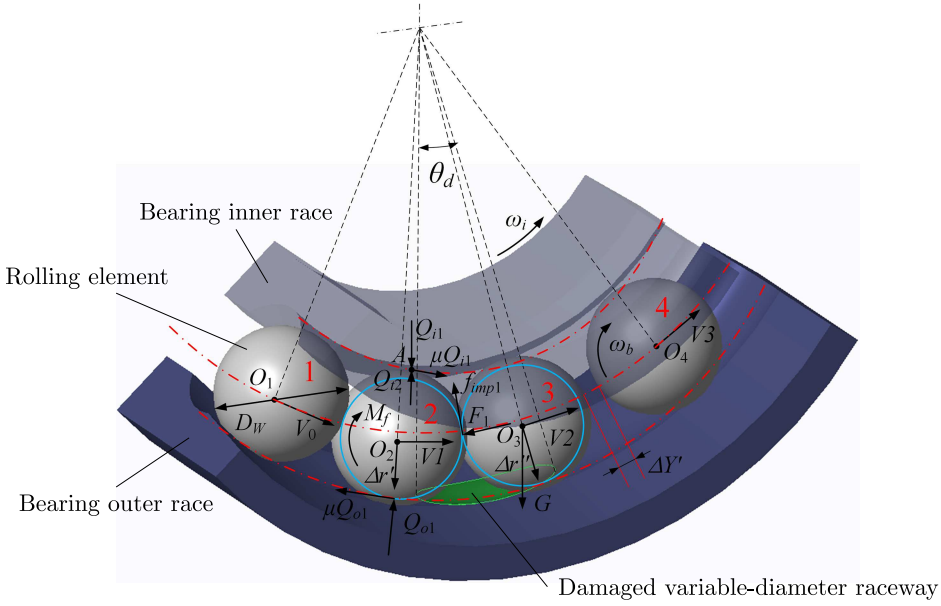

Fig. 2. Collision diagram for discrete failures

The rolling elements with the increasing velocity difference collide when $\Delta Y'$, and $\Delta Y' \geqslant 2\Delta Y$. Then the variable-diameter raceway undergoes a discrete failure, which is illustrated in Fig. 2. The radius of curvature $\Delta r'$ is

$$\Delta r' \leqslant \frac{D_w}{\Delta r \theta_d} 2(D_w - 2\Delta r)\theta_h + 2\Delta r \theta_d \tag{2.3}$$

Due to the short collision action time of the rolling element, there is no residual deformation after the collision, the collision deformation between the rolling element is regarded as elastic deformation. When the two rolling bodies collide at the speed V_1 and V_2, respectively, the relationship between deformation and velocity can be expressed as

$$\Delta V = \frac{d\delta_{imp}}{dt} = V_1 - V_2 \tag{2.4}$$

The force normal to the collision between the rolling bodies at any instant is

$$F_1 = m\frac{dV_1}{dt} = -m\frac{dV_2}{dt} = K_{bb}\delta_{imp}^{3/2} \tag{2.5}$$

The maximum collision deformation $d\delta_{imp}/dt$ is zero. Combined with Eq. (2.5), the integral and quadratic integral are solved to obtain the dynamic expression t^* of the deformation time in collision

$$t^* = \frac{\delta^*_{imp}}{\Delta V} \int \frac{d(\delta_{imp}/\delta^*_{imp})}{\sqrt{1 - (\delta_{imp}/\delta^*_{imp})^{5/2}}} \tag{2.6}$$

where δ^*_{imp} is the maximum deformation caused by collision of the rolling body.

After the moment of maximum compression t^* has been reached, deformation at the time of the rolling element collision can be fully recovered, and we obtain the total collision time T_c

$$T_c = 2t^* = 2\frac{\delta^*_{imp}}{\Delta V}\int_0^1 \frac{d(\delta_{imp}/\delta^*_{imp})}{\sqrt{1-(\delta_{imp}/\delta^*_{imp})^{5/2}}} = 2.94\frac{\delta^*_{imp}}{\Delta V} \tag{2.7}$$

The contact deformation of the rolling element affects the friction force at the collision point. The instantaneous force of rolling element 1 on the bearing inner ring is calculated by using the angular momentum conservation law

$$\Big(\frac{f_{imp}D_w}{2} - \mu Q_{t2}\frac{D_w}{2}\Big)(\omega_b - \omega'_b)T_c = \frac{1}{2}I\omega_b^2 - \frac{1}{2}I\omega_b'^2 \tag{2.8}$$

Rolling element 2 disconnects from the inner ring at the variable-diameter raceway, when rolling element 2 hits rolling element 1. We believe that the speed of rolling element 1 does not change at this time, and rotational speed $\omega'_b = \omega_b$, so we obtain

$$Q_{t2} = \frac{f_{imp}}{\mu} - \frac{2I\omega'_b\Delta V}{2.94\delta^*_{imp}\mu D_w} \tag{2.9}$$

where Q_{t2} is the load on the inner ring when the rolling body collides, μ is the coefficient of sliding friction, I is the moment of inertia of rolling elements.

3. Establishment of the vibration model under damage

In order to establish the proposed vibration model when the variable-diameter raceway is damaged, the time-varying stiffness, time-varying displacement and contact force of the rolling element rolling over the variable-diameter raceway are analyzed.

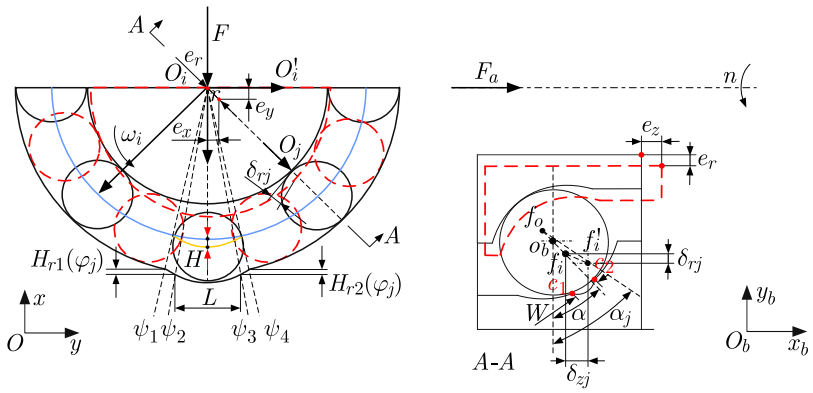

Fig. 3. Diagram of displacement change between the rolling element and inner ring

As shown in Fig. 3, when the rolling element passes along the variable-diameter raceway, the inner ring is detached. The rolling element position changes to produce the time-varying displacement H. The distance between the rolling element and the two contact points of the local variable-diameter raceway is $W(\varphi_j)$. The distance from the contact point of the rolling body to the beginning of the reducer raceway is $L(\varphi_j)$. The time-varying displacement of the rolling element in the variable-diameter raceway can be calculated from

$$\begin{aligned} L(\varphi_j) &= \frac{L}{2} - \Big(\frac{D_w}{2}\cos\alpha + \frac{d_m}{2}\Big)\tan\Big(\frac{3\pi}{2} - \mathrm{mod}(vp_j)\Big) \\ W(vp_j) &= W\sqrt{1 - \frac{[L(vp_j) - L/2]^2}{L^2/4}} \end{aligned} \tag{3.1}$$

and

$$
\begin{aligned}
H(\varphi_j) &= \sqrt{r_o^2 - W^2(\varphi_j)} - \sqrt{\Big(\frac{D_w}{2}\Big)^2 - W^2(\varphi_j)} + \frac{D_w}{2} - r_o \\
H_1(\varphi_j) &= \sqrt{r_o^2 - [W^2(\varphi_j) + w_d]^2} - \sqrt{\Big(\frac{D_w}{2}\Big)^2 - [W(\varphi_j) + w_d]^2} + \frac{D_w}{2} - r_o \\
&\qquad \psi_1 \leqslant \operatorname{mod}(\varphi_j 2\pi) < \psi_2 \\
H_{r1}(\varphi_j) &= H_r \frac{\operatorname{mod}\Big(\Big(\varphi_j - \frac{3\pi}{2} + \frac{\theta_d}{2}\Big), 2pi\Big)}{\psi_2 - \psi_1} \qquad \psi_2 \leqslant \operatorname{mod}(\varphi_j 2\pi) < \psi_3 \\
H_{r2}(\varphi_j) &= H_r \frac{\operatorname{mod}\Big(\Big(\frac{3\pi}{2} + \frac{\theta_d}{2} - \varphi_j\Big), 2pi\Big)}{\psi_4 - \psi_3} \qquad \psi_3 \leqslant \operatorname{mod}(\varphi_j 2\pi) < \psi_4
\end{aligned}
\tag{3.2}
$$

where $H(\varphi_j)$ is the time-varying displacement of the elliptical variable-diameter raceway without damage, see Fig. 3, the damage variable-diameter raceway is divided into three regions. $H_1(\varphi_j)$ caused by the damage width w_d and the damage depth h_d of the variable-diameter raceway is time-varying displacement of the element rolling on the damaged elliptical variable--diameter raceway in the $\psi_2 - \psi_3$ region. $H_{r1}(\varphi j)$ and $H_{r2}(\varphi_j)$ are the time-varying displacements of the rolling element in two sections of $\psi_1 - \psi_2$ and $\psi_3 - \psi_4$. The reason of time-varying displacement is that the contact point of the raceway with the conventional raceway extends outward after the damage of the raceway.

The damage of the variable-diameter raceway is related to the position of the contact point of the conventional raceway and the annular span angle. Thus the location of the two ends of damage can be expressed as

$$
\begin{aligned}
\psi_1 &= \frac{3\pi}{2} - \frac{1}{2}\Big(\theta_h + 4\arcsin\frac{w_d}{d_m + D_w\cos\alpha}\Big) \\
\psi_4 &= \frac{3\pi}{2} + \frac{1}{2}\Big(\theta_h + 4\arcsin\frac{w_d}{d_m + D_w\cos\alpha}\Big)
\end{aligned}
\tag{3.3}
$$

The total deformation of the rolling element and the collar is divided into two parts. It is the deformation amount of the rolling element when it rolls along the conventional raceway and the damaged variable raceway. The rolling element enters the $\psi_1 - \psi_4$ region and extrudes radially towards the outer ring. At this time, the reason for the decrease of time-varying displacement H is the contact deformation between the rolling element and the inner ring. Therefore, the total deformation δ_j for the time-varying displacement H segmentation function is given by the following formula

$$
\delta_j = \begin{cases} \sqrt{(e_x\cos\varphi_j + e_y\cos\varphi_j - H\cos\alpha)^2 + (e_z - H\sin\alpha)^2} & \psi_1 \leqslant \varphi_j \leqslant \psi 4 \\ \sqrt{(e_x\cos\varphi_j + e_y\cos\varphi_j)^2 + e_z^2} & \text{other} \end{cases}
\tag{3.4}
$$

The contact force Q_j between the rolling element and the raceway is related to the elastic contact displacement δ_j, which can be analyzed and calculated by the Hertz contact theory

$$
Q_j = K\sqrt{\delta_j^3}
\tag{3.5}
$$

where K is time-varying contact stiffness of the rolling element in the bearing.

The contact force of the inner ring is the combined force of each rolling element and the contact force of the inner ring when the rolling element is in the bearing region. The contact

force generated by deformation of the inner ring is decomposed along the coordinate axis xyz in the three directions, respectively. Its components $F = [F_{ix}, F_{iy}, F_{iz}]$ are

$$\begin{aligned} F_{ix} &= -\sum_{j=1}^{N} Q_j \cos\varphi_j \cos\alpha_j \qquad F_{iy} = -\sum_{j=1}^{N} Q_j \sin\varphi_j \cos\alpha_j \\ F_{iz} &= -\sum_{j=1}^{N} Q_j \sin\alpha_j \end{aligned} \tag{3.6}$$

The time-varying displacement of the damaged variable-diameter raceway is not enough to offset the contact deformation of the ring due to circumferential expansion. Therefore, we need to solve the contact stiffness K_{edge} and equivalent contact stiffness K_{edge} between the rolling element and the damaged variable-diameter raceway

$$\begin{aligned} K_{edge} &= \frac{4}{3}\frac{E_2(1-v_1^2)+E_1(1-v_2^2)}{E_1E_2}\sqrt[4]{\frac{D_w^2 r_o r}{(D_w+2r)(2f_o-D_w)}} \\ K'_{edge} &= 2\Big(K_{edge}\cos^2\frac{\beta_d}{2} + \frac{2T\sin[\rho\sin(\beta_d/2)\mp D_w/2]}{\rho D_w}\Big) \end{aligned} \tag{3.7}$$

where E_1 and E_2 are moduli of elasticity of the materials, ρ denotes the curvature radius of the trajectory of mass center of the rolling element, β_d is the support force angle and T is the rolling element support force.

After the equivalent contact stiffness of the rolling element and the damaged variable--diameter raceway is obtained, the time-varying contact stiffness K of the rolling element around the revolution can be obtained

$$K = \begin{cases} \left[K_i^{-2/3} + {K'_{edge}}^{-2/3}\right]^{-3/2} & \psi_1 < \mathrm{mod}(\varphi_j, 2\pi) < \psi_4 \\ \left[K_i^{-2/3} + K_o^{-2/3}\right]^{-3/2} & \text{other} \end{cases} \tag{3.8}$$

where K_i is the contact stiffness between the rolling element and the bearing inner ring, K_o is the contact stiffness between the rolling element and the outer ring in the conventional raceway.

Vibration characteristics of the bearing inner ring are caused by the contact collision between discrete failure of the rolling element and bearing. This collision occurs only in the radial plane of the bearing, without considering vibration caused by the extrusion of the bearing inner ring. Therefore, this paper establishes the vibration equation of the bearing inner ring, which simplifies calculation on the following assumptions.

- The contact deformation between the rolling element and raceway is considered, the plastic deformation caused by the contacting materials is ignored. We do not take into account microscopic slip friction in the contact region.
- The rolling element performs pure rolling motion on the raceway, the influence of gyro motion and sliding of the rolling body is ignored.
- We ignore the effect of lubricant film between the rolling element and raceway on motion and contact characteristics.
- The load and inner ring speed are stable without fluctuation during operation of the bearing.

From what has been discussed above, the time-varying stiffness, time-varying displacement and contact force of the rolling element rolling along the raceway with variable diameter are obtained. In order to establish the vibration model of the damaged raceway, the bearing is simplified as a spring-damping system. The vibration model of variable-diameter raceway damage is established.

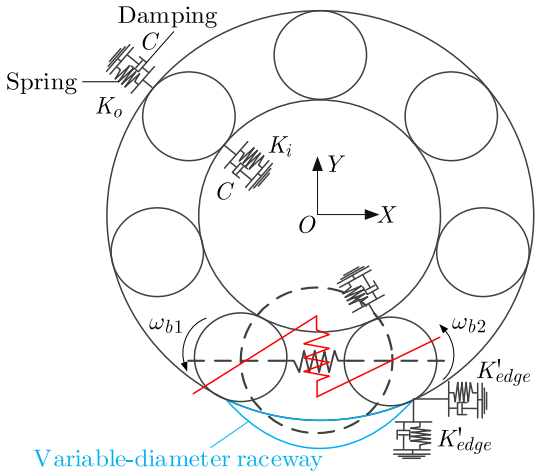

Fig. 4. Bearing vibration model

The vibration model of the ball bearing without the cage under the damage condition is shown in Fig. 4.

According to Newton's second law, based on variable-diameter raceway damage caused by time-varying displacement and time-varying stiffness excitation, a differential equation of vibration of the inner ring with the damaged variable-diameter raceway is established

$$\begin{aligned}
m_i\ddot{x}_i + c\dot{x}_i &= \lambda_j\Big(-\sum_{j=1}^{N} Q_j\cos(\phi_j\alpha)\cos\alpha_j\Big) + \Big(\frac{f_{imp}}{\mu} - \frac{2I\omega'\Delta V}{2.94\delta^*_{imp}\mu D_w}\Big)\cos\alpha\sin\psi_1\\
m_i\ddot{y}_i + c\dot{y}_i &= \lambda_j\Big(-\sum_{j=1}^{N} Q_j\sin(\phi_j\alpha)\cos\alpha_j\Big) + \Big(\frac{f_{imp}}{\mu} - \frac{2I\omega'\Delta V}{2.94\delta^*_{imp}\mu D_w}\Big)\cos\alpha\sin\psi_1 - F_r \qquad (3.9)\\
m_i\ddot{z}_i + c\dot{z}_i &= \lambda_j\Big(-\sum_{j=1}^{N} Q_j\sin\alpha_j)\Big) + \Big(\frac{f_{imp}}{\mu} - \frac{2I\omega'\Delta V}{2.94\delta^*_{imp}\mu D_w}\Big)\sin\alpha - F_a
\end{aligned}$$

where m_i are masses of the bearing inner ring and spindle, $\dot{x}_i$, $\dot{y}_i$ and $\dot{z}_i$ are velocities in the x, y and z directions of the inner circle, $\ddot{x}_i$, $\ddot{y}_i$ and $\ddot{z}_i$ are vibration accelerations in the x, y and z directions of the inner circle, F_a and F_r are the axial and radial loads borne by the bearing, λ_j denotes the control coefficient of contact deformation between the rolling elements.

4. Simulation research

Taking the angular contact ball bearing without the cage as an example, the radial load of the bearing is set to 500 N. Vibration characteristics of damaged variable-diameter raceway are found. The basic parameters of the damaged variable-diameter raceway bearing are shown in Table 1, and the material parameters of the bearing without the cage are shown in Table 2.

According to the discrete failure conditions obtained by Eq. $(2.1)_2$, the critical value of w_d is calculated. Figure 5 presents a relationship between the discrete distance of rolling elements and damage width of the variable-diameter raceway. Equation $(2.2)_2$ shows that the discrete spacing of the rolling element is 1.361 mm when the discrete failure occurs. In this paper, w_d is selected as 0.1 mm and 0.59 mm, MATLAB is used for programming, and the vibration equation is numerically solved by using the four-order Runge-Kutta algorithm with a fixed step.

Table 1. Basic parameters of damaged variable-diameter raceway bearings

Bearing parameters	Numerical values
Bearing inner diameter d_i [mm]	30
Bearing outer diameter d_o [mm]	62
Bearing width B [mm]	16
Section circle diameter d_m [mm]	46
Rolling element diameter D_w [mm]	9.525
Variable-diameter raceway length L [mm]	11.5
Variable-diameter raceway width W [mm]	3.5
Damage width w_d [mm]	0.1 (0.59)
Bearing contact angle α	15
Number of scrolling bodies N	10

Table 2. Bearing material parameters without the cage

Inner and outer rings	Values	Rolling element	Values
Modulus of elasticity of bearing steel [MPa]	$2.08 \cdot 10^5$	Modulus of elasticity of bearing steel [MPa]	$2.08 \cdot 10^5$
Poisson's ratio of bearing steel	0.3	Poisson's ratio of bearing steel	0.3
Bearing steel density [kg/mm^3]	$7.85 \cdot 10^{-6}$	Bearing steel density [kg/mm^3]	$7.85 \cdot 10^{-6}$

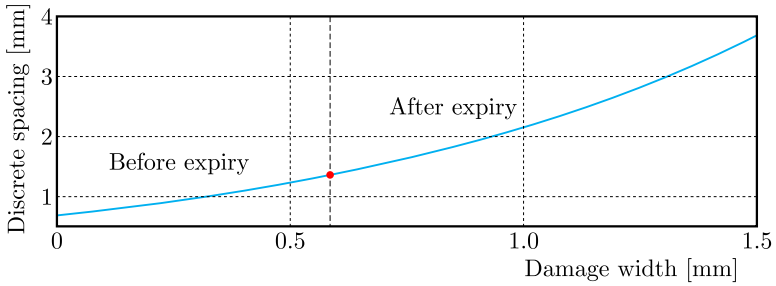

Fig. 5. Plot of bearing damage width versus discrete spacing

4.1. Simulation results and analysis of motion models

According to the differential equation of bearing vibration, the relation between the velocity and displacement of the inner ring and the damaged variable-diameter raceway is obtained. In Figs. 6 and 7, the bearing inner ring along the x-axis and y-axis direction displacement – velocity phase diagram is shown.

At three operating speeds, the inner ring of the bearing presents multiple closed rings along the x and y axes, and the bearing exhibits quasi-periodic motion, see Fig. 6.

As can be seen in Fig. 7, the phase diagram of the inner circle along the x- and y-axis directions does not repeat and fills a certain part of the phase space. Therefore, the inner circle motion is chaotic.

The displacement-velocity phase diagram of the inner ring at different rotational speeds is analyzed. When the damage width of the variable-diameter raceway is 0.1 mm, the inner ring motion is quasi-periodic under three rotational speeds. When the damage width of the variable--diameter raceway is 0.59 mm, the inner ring motion is chaotic at three speeds. With an increase of the damage width of the variable-diameter raceway, when the damage width is greater than or equal to 0.59 mm, the discrete failure of the rolling element occurs. The rolling element squeezes the inner ring to produce an instantaneous force, so motion of the inner ring changes from quasi-periodic to chaotic motion.

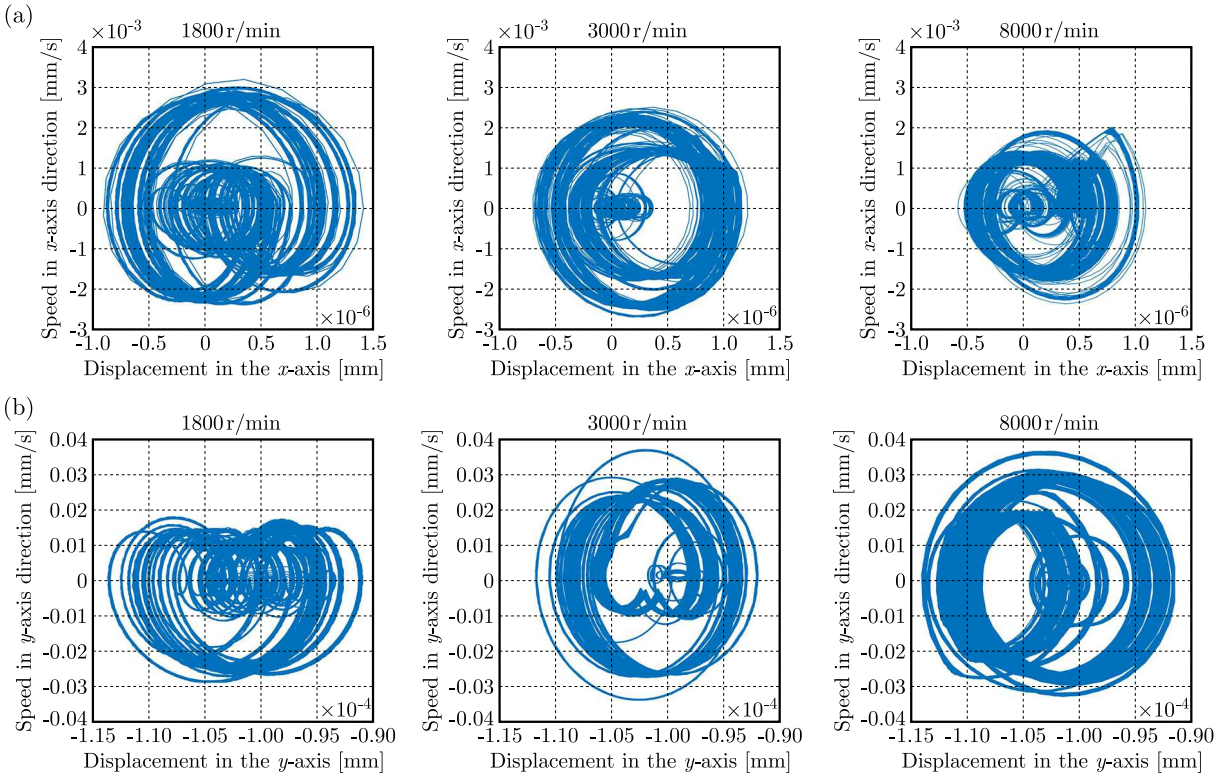

Fig. 6. Displacement-velocity phase diagram at 0.1 mm damage width of the variable-diameter raceway: (a) in x-axis direction, (b) phase in y-axis direction

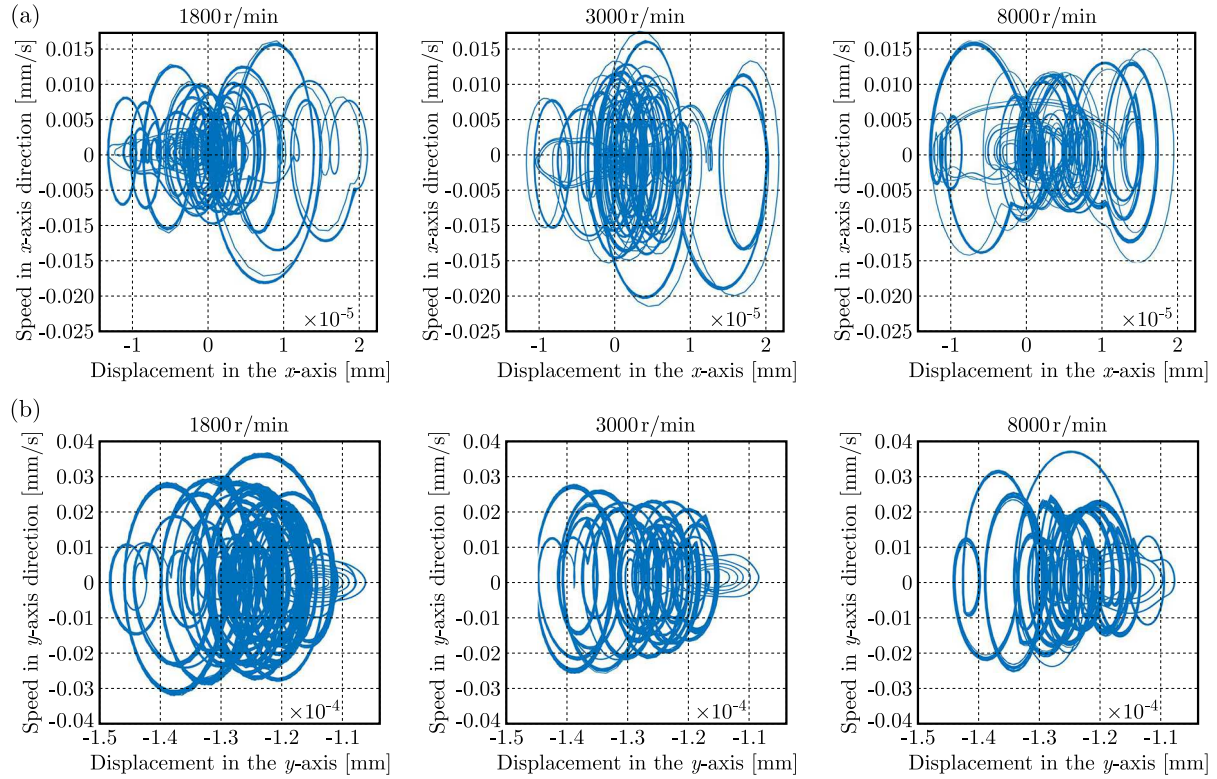

Fig. 7. Displacement-velocity phase diagram at 0.59 mm damage width of the variable-diameter raceway: (a) in x-axis direction, (b) phase in y-axis direction

After the law of motion of the rolling element is obtained, velocity changes of the two adjacent rolling elements passing along the variable-diameter raceway are simulated. Figure shows the velocity simulation result curve of the selected adjacent rolling elements.

It can be seen in Fig. 8a, the velocity change of the adjacent rolling elements in the conventional raceway is not obvious. The speed of roll 1 and 2 is kept at 1750-1780 mm/s. The radius of curvature of the damaged raceway changes and the velocity of two rolling elements fluctuates obviously. Figures 9 and 10 display the local magnification of motion within the range of 0.45-0.47 s, and the spacing curves of the adjacent rolling elements respectively.

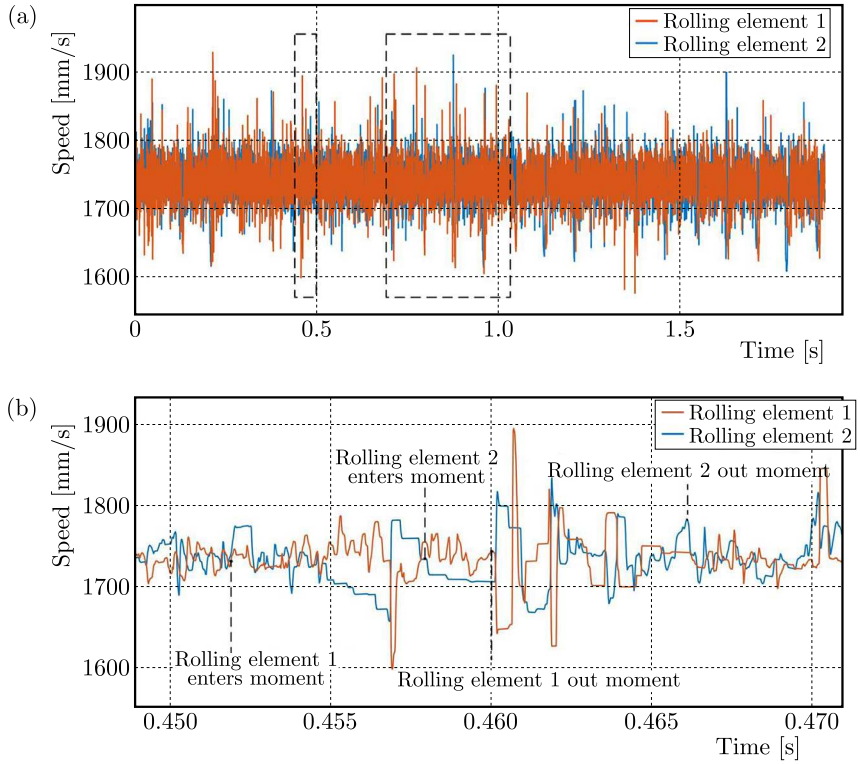

Fig. 8. Velocity curve: (a) damage to the adjacent rolling elements on the variable-diameter raceway, (b) local magnification curve of the adjacent rolling elements velocity

As shown in Fig. 8b, rolling element 1 enters the damaged variable-diameter raceway. Rolling element 1 is not detached from the damaged variable-diameter raceway. At this point, element 2 enters the damaged deceleration raceway. The time during which the rolling element passes along the damaged variable-diameter raceway is about 0.007 s. The damage width of the variable--diameter raceway increases. Although the acceleration between rolling elements decreases, there is still a time when the common acceleration is positive. When the acceleration difference between rolling element 3 and 2 is greater than that between rolling element 2 and 1, the distance between rolling element 1 and 2 and the distance between rolling element 2 and 3 both increase. As the acceleration becomes negative, the velocity starts to decrease. The velocity difference between rolling element 2 and 1 is getting smaller and smaller, which eventually leads the adjacent rolling element to the discrete failure.

The discrete spacing of adjacent rolling bodies reflects the degree of damage to the variable--diameter raceway and is represented by the ball spacing of three adjacent rolling elements. The effect of variable-diameter raceway damage on rolling element dispersion is studied, as shown in Fig. 9

The acceleration difference between rolling element 2 and 3 is larger than that between rolling element 2 and 1. The ball spacing between rolling element 2 and 3 varies greatly from Fig. 9a.

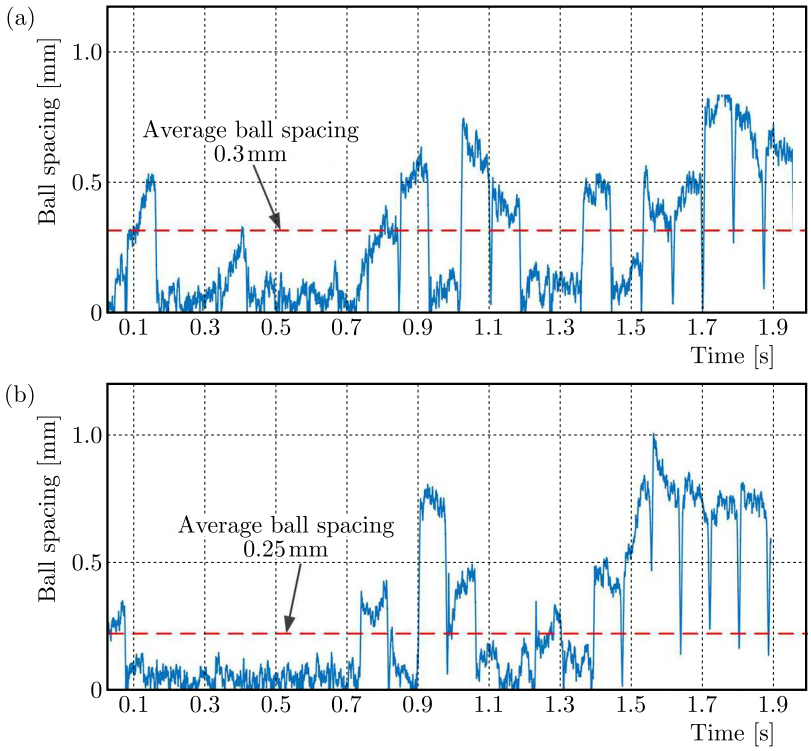

Fig. 9. Ball spacing between adjacent rolling bodies: (a) ball distance between rolling element 2 and 3, (b) ball distance between rolling element 1 and 2

The average pitch is about 0.3 mm. When the ball spacing of the rolling element is 0, adjacent rolling elements 3 and 2 collide. It can be seen from Fig. 9b that the ball spacing between rolling element 1 and 2 remains unstable. The average ball distance between the two rolling elements is about 0.25 mm, which is less than that of rolling elements 1 and 2. In the time range of 0.1 s-0.7 s, the ball spacing between rolling element 1 and 2 is always about 0. Adjacent rolling elements 1 and 2 collide.

4.2. Simulation results and analysis of vibration models

According to equations (3.9), the vibration acceleration of the inner ring is calculated. This time, the bearing speed is 1800 r/min. The damaged width of the variable-diameter raceway is 0.1 mm, 0.3 mm and 0.59 mm, respectively. The width of 0.1 mm, 0.3 mm and 0.59 mm represent the degree of mild, moderate and severe damage of the variable-diameter raceway, respectively.

Figure 10 shows the vibration acceleration curve with a damaged width of 0.1. The amplitude of acceleration has obvious periodic characteristics in Fig. 10a. It shows that the amplitude is stable and the rolling elements are loaded uniformly. It can be seen from Fig. 10b that the maximum amplitude of the acceleration curve is about 70 m/s^2, and the interval between the two peaks is about 0.006 s.

The amplitude of vibration acceleration of the bearing increases with an increase of the damage width, but changes periodically in Fig. 11a. The amplitude change is small. In the local enlargement of Fig. 11b, the maximum value of acceleration curve change caused by the damaged raceway is about 100 m/s^2. At this time, the rolling element remains discrete in the movement process. A_1 and B_1 respectively represent vibration values of the rolling element when it enters and leaves the variable-diameter raceway. The interval between the two peaks is about 0.006 s, which is the same as monopulse vibration with mild damage. With an increase

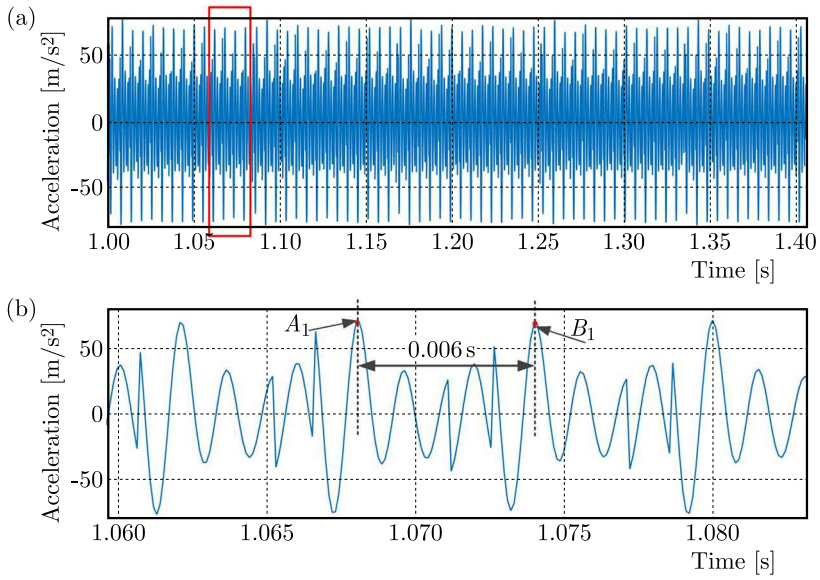

Fig. 10. $w_d = 0.1$ mm: (a) vibration acceleration curve, (b) partial enlarged drawing

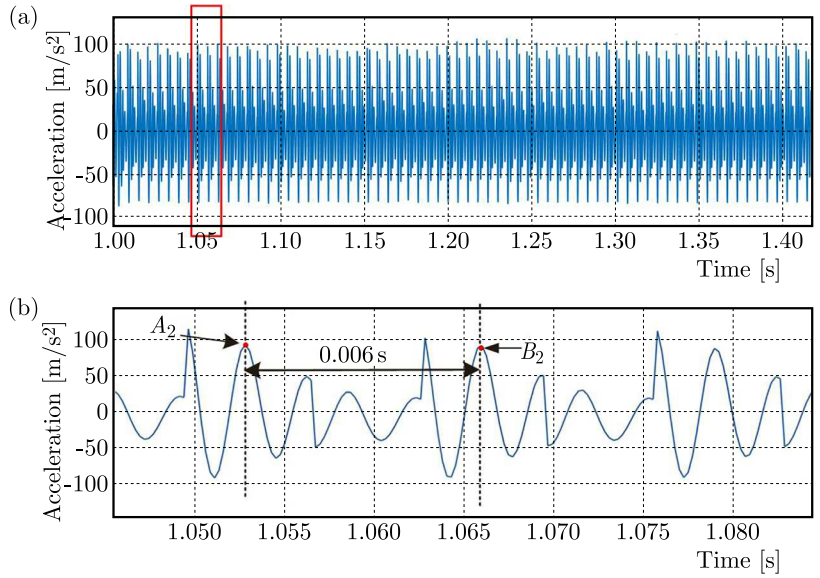

Fig. 11. $w_d = 0.3$ mm: (a) vibration acceleration curve, (b) partial enlarged drawing

of damage, the rolling element generates an impact excitation at the variable-diameter raceway and the vibration amplitude increases.

As shown in Fig. 12a, the maximum change in the acceleration curve due to damage to the reducer raceway is approximately 100 m/s^2. There are several locations in the diagram where the peak acceleration is approximately zero, indicating that 14 rolling elements are packed together at this time. Figure 12b shows that when the damage width is 0.59 mm and the circumferential span angle of the damaged variable-diameter raceway is 26.28°, p_1' and p_2' are at the moment when the rolling element enters and leaves the damaged variable-diameter raceway. Due to the increase of the damage width of the variable-diameter raceway, the number of rollers changes, and the collision force between the rollers causes an instantaneous force act on the roller on the bearing inner ring. Therefore, the acceleration amplitude of the inner ring increases significantly when the damage width of the variable diameter raceway is 0.59.

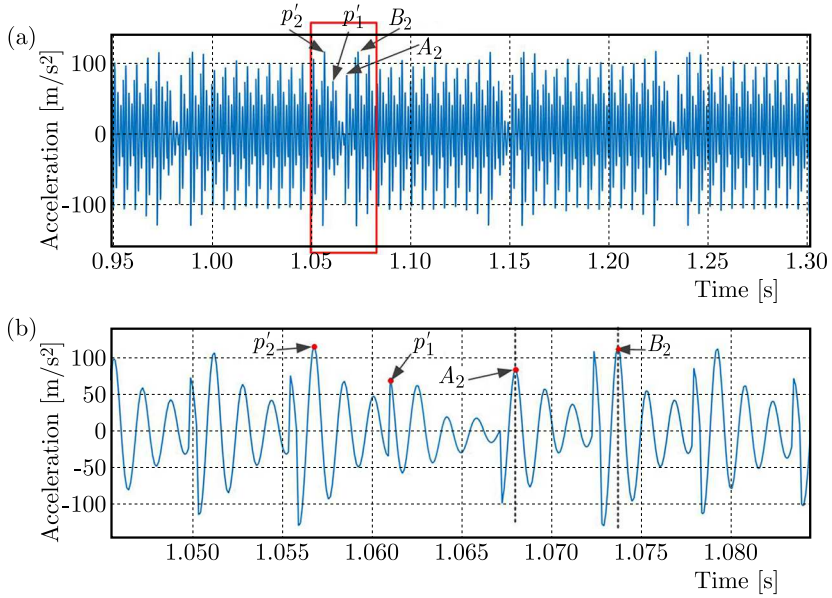

Fig. 12. $w_d = 0.59$ mm: (a) vibration acceleration curve, (b) partial enlarged drawing

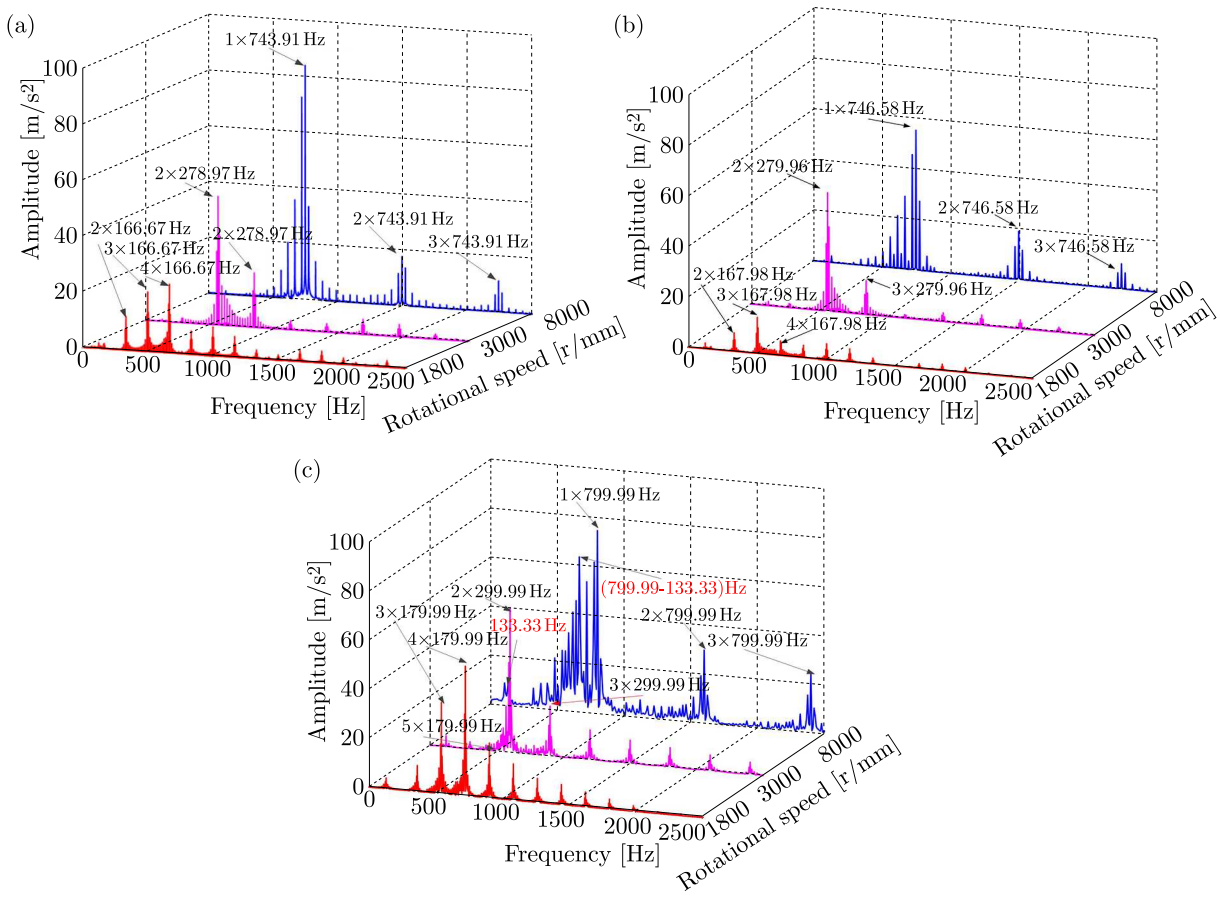

Fig. 13. Frequency-domain waterfall diagram: (a) $w_d = 0.1$, (b) $w_d = 0.30$, (c) $w_d = 0.59$

In order to further investigate the effect of different speeds on vibration in the frequency domain, three speeds of 1800 r/min, 3000 r/min, and 8000r/min are selected for numerical simulation in this paper.

Figure 13 shows that the amplitude of vibration acceleration of the bearing inner ring increases significantly with an increase of rotational speed. However, the vibration amplitude of mild damage is higher than that of moderate damage under the condition of low and high speed. Although most of the rolling elements are dispersed at this time, there is still a small part of the rolling elements in contact, which does not affect motion of the bearing. Although most of the rolling elements have been dispersed under the influence of rotational speed, there is still a small part of the rolling bodies in contact with each other, which does not affect motion of the rolling bodies. The corresponding frequency peak of each rotational speed is approximately a multiple relationship of its theoretical frequency, and the bearing rollers can be dispersed at three rotational speeds at $w_d = 0.1$ and $w_d = 0.3$. The corresponding frequency amplitudes at each speed are greater than the theoretical values of $w_d = 0.59$. Moreover, asymmetry of the inner ring rotation center intensifies with an increase of rotational speed. It results in a larger frequency characteristic peak of bearing vibration, which leads to the aggravation of bearing vibration.

The analysis of the time and frequency domain shows that vibration of the inner ring of the ball bearing without the cage becomes more complex, and the vibration amplitude increases with an increase of damage width.

5. Experimental research

The outer ring with a variable-diameter raceway machined by EDM is installed on the ball bearing without the cage. The experiment is carried out on a T10-60 machine. Vibration data of the ball bearing without the cage under different working conditions are measured. The T10-60 machine is shown in Fig. 14a. The outer ring of the ball bearing without the cage is shown in Fig. 14b. The experimental scheme is shown in Table 3.

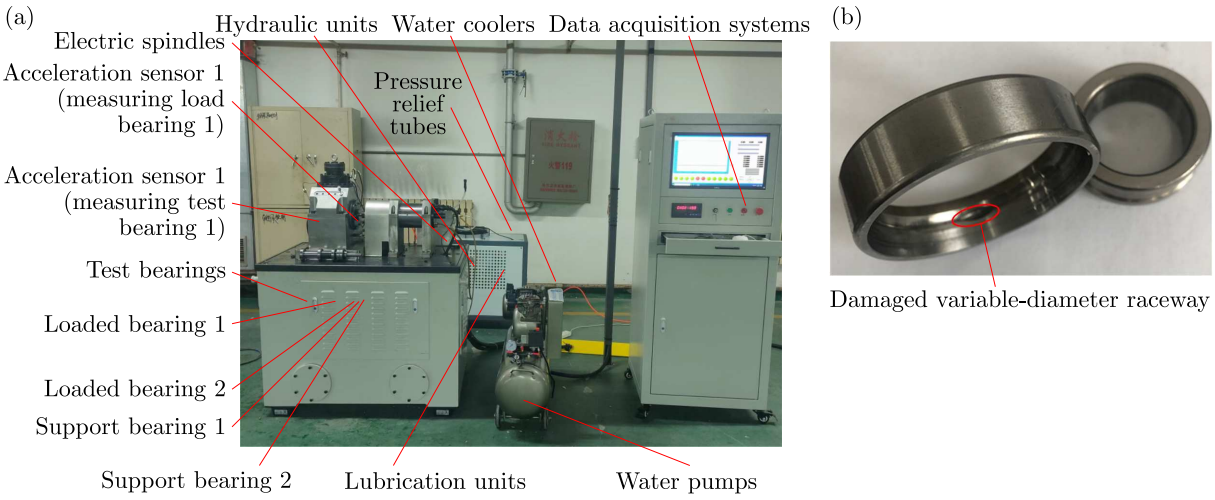

Fig. 14. Experiment equipment: (a) model T10-60 bearing vibration tester, (b) diagram of the damaged variable-diameter raceway

The vibration data was collected after the bearings entered steady operation. The vibration curves of the bearings were given for radial forces of 300 N, 500 N and 800 N at a speed of 1800 r/min without the ball bearings cage, as shown in Fig. 15.

As shown in Fig. 15, the amplitude range of the vibration curve of the damaged variable--diameter raceway bearing under the action of a 300 N radial force is about (1.2-1.5) mm/s^2. The amplitude range of the vibration curve under the action of a 500 N radial force is (1.25-1.45) mm/s^2. There is almost no change compared with the bearing vibration under the

Table 3. Experimental scheme

Rotational speed [r/min]	1800			3000	8000
Radial load [N]	300	500	800	500	500
Lubrication method	Oil lubrication				
Mounting method	Reducing raceway at lowest point of load area				
Damage to variable-diameter raceway position	Outer ring				

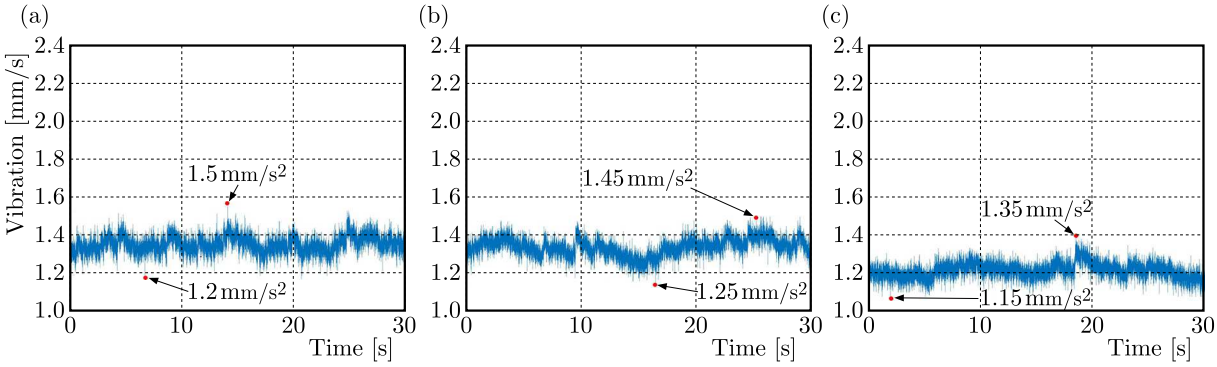

Fig. 15. Vibration acceleration test curve for bearings at 1800 r/min: (a) $F_r = 300$ N, (b) $F_r = 500$ N, (c) $F_r = 800$ N

radial force of 300 N. For a 800 N radial force, the amplitude is (1.15-1.35) mm/s^2. Compared with 300 N and 500 N radial forces, the bearing vibration is slightly reduced. The load has little influence on the vibration amplitude, which can be seen from the vibration curves of bearings under three loads.

In order to further verify the influence of speed of the damaged variable-diameter raceway bearing on vibration, the operating speeds of 3000 r/min and 8000 r/min were selected, and the vibration data of the damaged variable-diameter raceway were measured under the same radial load of 500 N, as shown in Fig. 16.

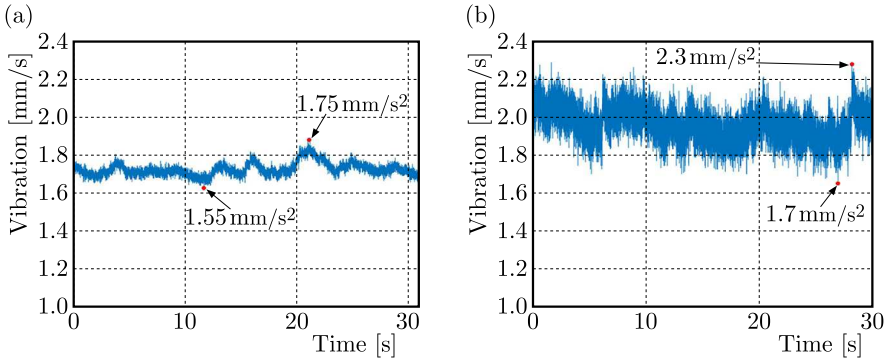

Fig. 16. Vibration acceleration experiment curve of the bearing: (a) speed is 3000 r/min, (b) speed is 8000 r/min

It can be seen from Fig. 16 that the vibration acceleration range of the bearing at 3000 r/min is (1.55-1.75) mm/s^2. The vibration acceleration range of the bearing at 8000 r/min is (1.7--2.3) mm/s^2. Obviously, with the increase of rotational speed, vibration of the damaged variable--diameter raceway intensifies. Compared with Fig. 15b, the radial load is the main factor affecting the vibration amplitude. This shows that the operational speed has a significant correlation with vibration of the damaged variable-diameter raceway.

The precision electronic analytical balance BSM220.4 is used in this paper, and the measurement accuracy is 0.1 mg. In order to ensure the weighing accuracy, the experimental samples are cleaned by ultrasonic waves for 10 minutes. Then they are blown dry and weighed. According to the literature (Zhao *et al.*, 2021), it can run for 300 hours under dry friction. Table 4 shows the amount wear extent of the damaged variable-diameter raceway at the same time and different speed.

Table 4. Wear extent at different speeds

Bearing number	Rotate speed [r/min]	Initial mass [g]	Damaged mass [g]	Wear extent [mg]
1	1800	90.1779	90.1727	2.2
2	3000	89.7026	89.6995	3.1
3	8000	89.8427	89.8303	12.4

The wear degree of the raceway becomes worse with an increase of rotational speed. The wear extent at high speed is much higher than that at middle and low speed, which may be due to the violent collision force of the rolling element at high speed. Wear occurs on the surface of rolling elements.

The experimental results for three rotational speeds show that the vibration amplitude of the bearing without the cage in the damaged variable-diameter raceway does not change significantly with the load. But vibration intensifies with an increase of rotational speed. This is consistent with the comparison results of the damaged frequency-domain waterfall diagram in the simulation.

6. Conclusions

The damage of the variable-diameter raceway leads to an increase of bearing vibration, which will accelerate the failure of the machine. This paper analyzes the influence of the damaged variable--diameter raceway on dynamic characteristics of the rolling element. The vibration equation of the ball bearing without the cage is established. Vibration of the damaged variable-diameter raceway is studied by numerical solution, simulation analysis and experiment. The specific conclusions are as follows:

- With deterioration of the variable-diameter raceway, the vibration amplitude of the bearing increases obviously. Vibration fluctuation caused by the discrete failure of the rolling element indicates that the collision force between rolling elements is the main factor resulting in violent vibration.
- The vibration acceleration of the bearing in the conventional raceway is less than that in the variable raceway. The contact point changes from point 1 to point 2 when the rolling element enters the variable-diameter raceway. This leads to time variation of displacement and contact stiffness.
- The velocity-displacement phase diagram is analyzed. Damage visibility of the local variable-diameter raceway increases. Due to the discrete failure of the rolling element, an instantaneous force is generated in the rolling element extrusion inner ring. Therefore, the inner-loop motion is transformed from quasi-periodic to chaotic motion.
- The local variable-diameter raceway is slighty damaged and does not affect the dispersion effect. Vibration occurs only at the theoretical frequency or its multiple. However, when damage of the local variable-diameter raceway is large, the dispersion effect is affected. Vibration is greater than that of the theoretical frequency value or its multiple.

The frequency variation of damage can be used as the basis for monitoring the state of the machine system in the future.

Acknowledgments
This work was supported by the National Natural Science Foundation of China(51875142), China.

References

1. Behzad M., Bastami A.R., Mba D., 2011, A new model for estimating vibrations generated in the defective rolling element bearings, *Journal of Vibration and Acoustics – Transactions of the ASME*, **133**, 4, 041011
2. Cui L.L., Jin Z., Huang J.F., Wang H.Q., 2019, Fault severity classification and size estimation for ball bearings based on vibration mechanism, *IEEE Access*, **7**, 56107-56116
3. Fan J., Cui W., Han Q.K., 2017, Vibration signal modeling of a localized defective rolling bearing under unbalanced force excitations, *Journal of Vibroengineering*, **19**, 7, 5009-5019
4. Khanam S., Dutt J.K., Tandon N., 2015, Impact force based model for bearing local fault identification, *Journal of Vibration and Acoustics – Transactions of the ASME*, **137**, 5, 051002
5. Liu J., Tang C.K., Shao Y.M., 2019, An innovative dynamic model for vibration analysis of a flexible rolling element bearing, *Mechanism and Machine Theory*, **135**, 27-39
6. Liu J., Wu H., Shao Y.M., 2018, A theoretical study on vibrations of a ball bearing caused by a dent on the races, *Engineering Failure Analysis*, **83**, 220-229
7. Liu Y.Q., Chen Z.G., Wang K.Y., Zhai W.M., 2022, Surface wear evolution of traction motor bearings in vibration environment of a locomotive during operation, *Science China – Technological Sciences*, **65**, 4, 920-931
8. McFadden P.D., Smith J.D., 1984, Model for the vibration produced by a single point-defect in a rolling element, *Journal of Sound and Vibration*, **96**, 1, 69-82
9. Parmar V., Saran V.H., Harsha S.P., 2021, Effect of dynamic misalignment on the vibration response, trajectory followed and defect-depth achieved by the rolling-elements in a double-row spherical rolling-element bearing, *Mechanism and Machine Theory*, **162**, 104366
10. Shah D.S., Patel V.N., 2019, A dynamic model for vibration studies of dry and lubricated deep groove ball bearings considering local defects on races, *Measurement*, **137**, 535-555
11. Xi S.T., Cao H.R., Chen X.F., 2019, Dynamic modeling of spindle bearing system and vibration response investigation, *Mechanical Systems and Signal Processing*, **114**, 486-511
12. Yang Y., Ouyang J., Wu X.L., Jin Y.L., Yang Y.R., Cao D.Q., 2019, Bending-torsional coupled vibration of a rotor-bearing-system due to blade-casing rub in presence of non-uniform initial gap, *Mechanism and Machine Theory*, **140**, 170-193
13. Yang Y.Z., Yang W.G., Jiang D.X., 2018, Simulation and experimental analysis of rolling element bearing fault in rotor-bearing-casing system, *Engineering Failure Analysis*, **92**, 205-221
14. Zhao Y.L., Wang Q.Y., Wang M.Z., Pan C.Y., Bao Y.D., 2022, Discrete theory of rolling elements for a cageless ball bearing, *Journal of Mechanical Science and Technology*, **36**, 4, 1921-1933
15. Zhao Y.L., Zhang J.W., Zhou E.W., 2021, Automatic discrete failure study of cage free ball bearings based on variable-diameter contact, *Journal of Mechanical Science and Technology*, **35**, 11, 4943-4952
16. Zheng L.K., Xiang Y., Sheng C.X., 2021, Nonlinear dynamic modeling and vibration analysis of faulty rolling bearing based on collision impact, *Journal of Computational and Nonlinear Dynamics*, **16**, 6, 061001

Manuscript received May 28, 2022; accepted for print October 3, 2022